Int J Adv Manuf Technol (2017) 93:3541–3550
DOI 10.1007/s00170-017-0753-8

ORIGINAL ARTICLE

Dual-drive long-travel precise positioning stage of grating ruling engine

JingShu Wang[1] · **Bayanheshig**[2] · **ChangAn Zhu**[3]

Received: 7 October 2016 / Accepted: 26 June 2017 / Published online: 21 July 2017

Abstract The presented dual-drive long-travel precise positioning stage is employed in grating ruling engine and capable of extended travel and high precision. Based on the characteristic of grating ruling engine, a dual-drive positioning system is developed. The primary positioning stage is an open-loop system and designed to obtain long-travel range. The secondary positioning stage with a control system can guarantee the positioning precision being less than 10 nm. After modeling the fine positioning system, a single-neuron-based PID controller is employed to implement the control system. The experiment results demonstrate that in the long-travel mode, the stage is capable of performing positioning with an extended move range and accuracy being less than 10 nm. Meanwhile, in the short-travel mode, the stage performs positioning with a limited range of 120 μm and accuracy being less than 7 nm. The main sources of the positioning deviation including clearance, vibration, and the measurement error are analyzed in detail.

✉ JingShu Wang
donot@cqut.edu.cn

Bayanheshig
bayin888@sina.com

ChangAn Zhu
Changan@ustc.edu.cn

[1] School of Mechanical Engineering, Chongqing University of Technology, Chongqing 400054, China

[2] Changchun Institute of Optics, Fine Mechanics and Physics, Chinese Academy of Sciences, Changchun 130033, China

[3] Department of Precision Machinery and Precision Instrumentation, University of Science and Technology of China, Hefei 230027, China

Keywords Grating ruling engine · Positioning stage · Dual drive · Positioning mode · Positioning error

1 Introduction

As the core component of spectrum instruments, the diffraction grating is widely applied in many fields, such as astronautics, astronomical observation, bioresearch, and defense construction. The diffraction grating featured of high accuracy and large area must be produced by mechanical ruling engine. The major components of the grating ruling engine are the positioning system and the ruling system. This paper focuses on the precise positioning system of the grating ruling engine.

Recent development of high performance mechatronic systems, such as scanning probe microscopy, precise machine tools, optical components manufacturing, and biomedical engineering, results in the requirement of precise positioning stages. Due to the wild applications of the precise positioning stage, there are different emphases for their respective categories.

The first class is comprised of probe-type measuring machine, atomic arrangement, and biomedical engineering, such as the scanning tunneling microscope (STM), the atomic force microscope (AFM), and the magnetic force microscope (MFM) [1–3]. These devices focus on the microstructure of the test piece, therefore the positioning stage with performance at 10 nm (or less) scale and maximum range of approximately 30 μm is required. Another category demands the positioning stage which can provide a large travel range with nanoscale resolution. The nano-coordinate measuring machine, the grating ruling engine, the IC stepper machine, and the precise manufacturing machine all belong to this category [4–6]. These devices require travel range of several centimeters and resolution of approximately 10 nm. The precise

positioning stage of the grating ruling engine belongs to the long-travel category.

Since the precise positioning system plays a crucial role in many nanotechnology applications, more and more attentions of the scholars and experts have been drawn in recent years. According to the different drive modes, positioning systems can be divided into friction-stages, inchworm-stages, and elastic deformation-stages.

Considering the friction-stages, the advantage of this type is the long-travel range. Nevertheless, the friction-drive stages have shortcomings such as complicated setup and low loading ability. Lee and Kim utilized direct current (DC) motor and mechanism of H-shape to drive the coarse stage [7]. The device was capable of working, ranging up to 200 mm and positioning reproducibility less than 20 nm. Fan and Lai designed a linear positioning system driven by an ultrasonic motor and built a fuzzy cerebella model articulation controller to accomplish the purpose of an intelligent nano-positioning control [8]. A piezoelectric-driven Scott-Russel linear micropositioner with the slider driven by the stick-slip effect of friction was presented by Chang and Li. [9] The measured step size of the micropositioner ranged from 50 nm to 120 μm, and the speed was up to 2.5 mm/s. Kim and Liu et al. also adopted the stick-slip friction principle to drive precision linear stages [10, 11].

The inchworm-screw is another possible candidate for long-travel nanopositioning. The drawbacks include backlash, wear, and complicated control mechanism. Ito et al. researched a ball screw-driven precision positioning stage with specifications of ±10 μm in accuracy and 100 ms in setting time for positioning amplitude of 5 mm [12]. Cheng et al. studied a positioning stage based on ball screw and robust control. The standard deviation of positioning was less than 5 nm, and the travel was up to 15 mm [13]. Liu et al. designed a dual-axis positioning stage with travel range of 300 mm × 300 mm and positioning accuracy of 10 nm [14]. Li et al. and Shiau also made use of the inchworm-screw to drive nanopositioning stages [15, 16].

The movement of the elastic deformation stages is due to the elastic deformation of the flexure. The flexure hinges are often employed to replace conventional joints owning to the advantages of no friction, no backlash, no wear, and compact structure. The disadvantage is the limited travel range. Chu and Fan applied material elastic deformation principles and utilized a stack-piezoelectric actuator to design a linear micropositioner. The stage could perform a scanning motion over a displacement range of 10 mm with the resolution higher than 10 nm [17]. Hwang et al. presented an in-plane XYθ positioning stage by means of the flexure notch hinges. The resolutions were ±0.15 nm, ±0.15 nm, and ±0.15 μrad for X-axis, Y-axis, and rotational motion, respectively [18]. Other than these researchers, many scholars as well employed flexure joints for nanopositioning [19–22].

By analyzing the survey of various precise positioning systems, it can be concluded that the inchworm-stage can reach a long travel but is hard to control. On the contrary, the elastic deformation-stage is straightforward to control but with a limited travel range. By combining the two actuators with an appropriate control strategy, the disadvantages of one actuator can be compensated by the merits of the other.

The positioning stage of the grating ruling engine presented in this paper is a dual-drive long-travel stage. The precise positioning stage is composed of two stages, which are driven by inchworm and piezoelectric ceramic, respectively. As the experimental results show, an integrated performance of both large travel and high precision can be achieved.

2 Positioning system of grating ruling engine

The actual object of the grating ruling engine is shown in Fig. 1a. The grating ruling engine comprises a positioning system and a ruling system. As shown in Fig. 1b, during the grating ruling process, the positioning system carrying the stage which is relatively heavy moves in one direction, while the ruling system containing the tool post which is relatively light implements reciprocating movement. The grating groove is the profile synthesis of the two movements. One reciprocating motion of the ruling system realizes one grating groove. This working type is featured of simple structure and smooth operation.

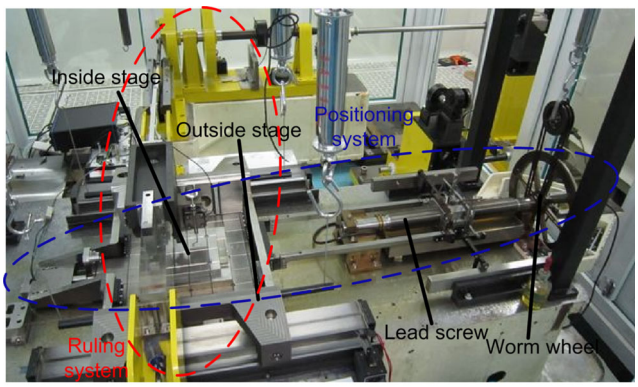

(a) The grating ruling engine

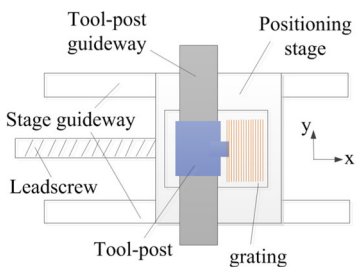

(b) The working mode of the grating ruling engine

Fig. 1 The structure and the working mode of the grating ruling engine

Table 1 Specifications of the coarse system

Pitch of ball screw	1 mm
Worm gearing transmission ratio	600:1
Stroke of ball screw	560 mm

This paper focuses on the precise positioning stage of grating ruling engine. Due to manufacturing optical grating, in each period, the precise positioning stage should move for certain distance as grating constant, then stop and wait for the ruling system to rule one line of grating. According to the features of manufactured grating, the positioning stage is characterized by long travel and high accuracy. Therefore, the dual-drive positioning system comprised of a coarse positioning system and a fine positioning system is designed. The coarse positioning system driven by the ball screw is designed to expand the travel range, while the piezoelectric-drive fine positioning system is applied to obtain high accuracy.

2.1 The dual-drive positioning system

The coarse positioning system consists of a primary stage, a guide rail, screw-nut pair, worm-gear pair, and a servo motor. The primary stage can move along the guide rail. The coarse system is characterized by large travel but poor accuracy and slow response. The positioning range of the coarse system is as long as 500 mm.

The parameters of the coarse system are listed in Table 1. The coarse system driven by the ball screw is an open-loop system. When the motor completes one turn, the rotation angle of the worm wheel is $2\pi/600$, then the displacement of the secondary stage caused by the movement of the screw is 1/600 mm, namely 1.667 μm. The positioning accuracy of the coarse system relies on the precision of the machinery parts and the rotation accuracy of the motor. Owning to the machining errors and function errors, deviations of hundreds of nanometers even a few micrometers are brought into the locating process of the coarse system. The deviations will be compensated in the fine positioning system.

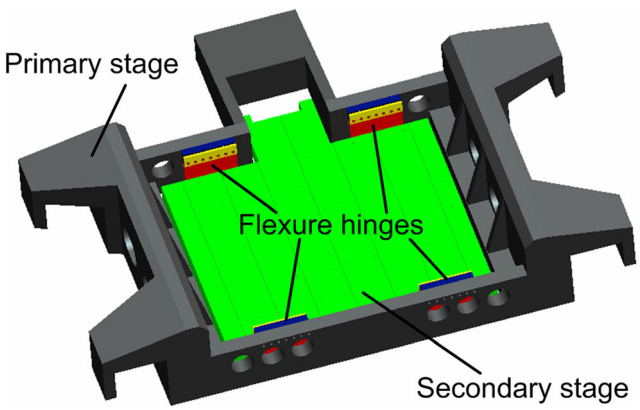

Fig. 2 The schematic illustration of the stages

Table 2 The technical data of the piezo-actuator

Type	PAHL120/20
Motion	120 μm
Pre-load	350 N
Stiffness	30 N/μm
Resonant frequency	5 kHz
Resolution open loop	0.15 nm

As the Fig. 2 shows, the secondary stage is fastened to the primary stage by four flexure hinges. The fine positioning system includes a secondary stage, a piezoelectric actuator, and four flexure hinges. The piezoelectric actuator with one end fastened to the primary stage clings to the secondary stage through the pre-loaded springs.

The grating to be ruled is installed on the secondary stage which driven by the piezoelectric actuator. In order to reach high positioning accuracy, the fine positioning system should be a closed-loop system. A dual-frequency laser interferometer is employed to measure the location error of the secondary stage. Based on the error, the location of the grating can be adjusted by the piezoelectric actuator. The adjustment process is realized by a control system in section 2.2.

The piezo-actuator, PAHL120/20, produced by the Piezosystem Jena Company, has been chosen as the secondary actuator. Table 2 lists the parameters of the piezoelectric ceramic. The measurement system, produced by Agilent Company, is composed of 10715A differential interferometer and N1231 laser board. The technical data are listed in Table 3.

The whole structure of the dual-drive positioning system is designed to meet Abbe's principle of alignment. In the coarse positioning system, the axis of lead screw is coincident with the working face of the grating. For the fine positioning system, after completing the assembly, the upper surface of the secondary stage will keep in the same horizontal plane with the top of the slide guide.

As shown in Fig. 3, the three-dimensional simulation model of the dual-drive positioning system is created, and dynamic simulation is carried out before we determine final parameters of the system.

Table 3 The technical data of the measurement system

Hardware update rate	20 MHz
Resolution	0.15 nm
Maximum stage velocity	1000 mm/s

Before the setup of control system, we should first understand characteristics of controlled object, namely, the fine positioning system. After parameters identification, an ARX model is applied to describe the system as follows:

$$A(z^{-1})y(k) = B(z^{-1})\,u(k)$$

$$\begin{cases} A\ (z^{-1}) = 1 - 1.384z^{-1} + 0.557z^{-2} + 0.2863z^{-3} - 0.6843z^{-4} + 0.5743z^{-5} - 0.2098z^{-6} \\ \qquad\quad - 0.07043\ z^{-7} + 0.03448\ z^{-8} + -0.3324\ z^{-9} + 0.3163\ z^{-10} \\ B(z^{-1}) = 0.08465 \end{cases}$$

In the model, u is the input of the piezoelectric actuator and y is the displacement of the secondary stage. As shown in Fig. 4, the output of the ARX model is in good agreement with the location data, especially in the overshoot part. This ARX model can describe the fine positioning system to some extent. After many types of controller based on the model have been simulated, the single-neuron-based proportional–integral-derivative (PID) controller is characterized with simple construction and perfect performance. So the final selection is this type.

2.2 The control system

In the fine positioning process, the control system adjusts the length of the piezoelectric actuator according to the position error of the secondary stage. The real-time displacement of the secondary stage will be imported into the control system. Both the sampling frequency of the interferometer and the control frequency of the system is 1 KHz.

The algorithm adopted in the control system is the single-neuron-based PID controller. The features of the PID controller include simple calculation, strong robustness, and easy realization. The single-neuron network is a simple network with only one neuron, so the calculation is simple and easy, too. As an adaptive algorithm, the single-neuron network is characterized by adaptability. Synthesizing the advantages of the two algorithms, the single-neuron-based PID controller utilizes the single-neuron network to adjust the parameters of the PID controller. The calculation formulate is shown below:

$$u(k) = u(k-1) + K\sum_{i=1}^{3} w_i'(k)x_i(k) \tag{1}$$

$$w_i'(k) = w_i(k) \Big/ \sum_{i=1}^{3} |w_i(k)|, i = 1,2,3 \tag{2}$$

$$w_i(k) = w_i(k-1) + \eta_i u(k)x_i(k), i = 1,2,3 \tag{3}$$

where $[x_1(k)\ \ x_2(k)\ \ x_3(k)] = [e(k)\ \ e(k) - e(k-1)\ \ e(k) - 2e(k-1) + e(k-2)]$, and e denotes the deviation of the secondary stage which is measured by the interferometer. η is the learning rate of the single neuron network. u and K denote the input of the controller and network's scale factor, respectively.

The block diagram of the controller is presented in Fig. 5. Based on the feedback displacement of the secondary stage, the single-neuron-based PID controller calculates the compensation length and sends it to the piezoelectric actuator.

3 System characteristics

The positioning experiment without ruling operation is conducted to analyze the characteristics of the positioning system.

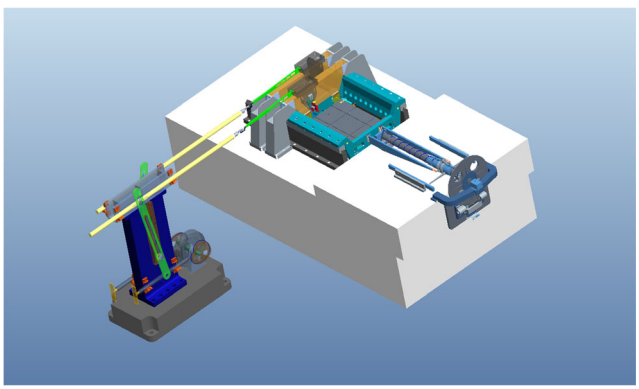

Fig. 3 The simulation model of the dual-drive positioning system

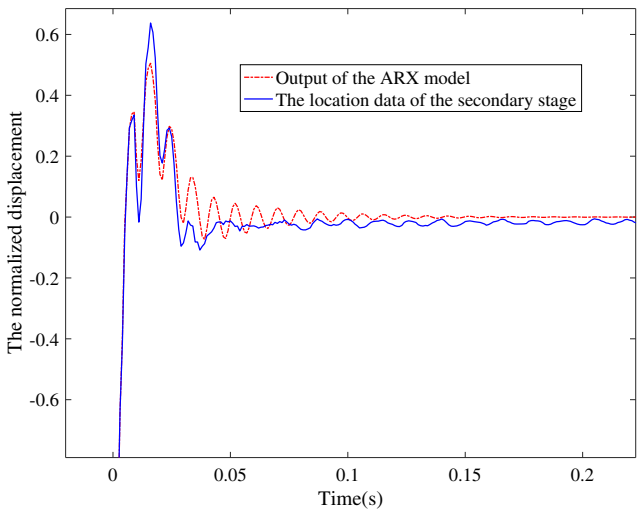

Fig. 4 The output of the ARX model and the real fine system

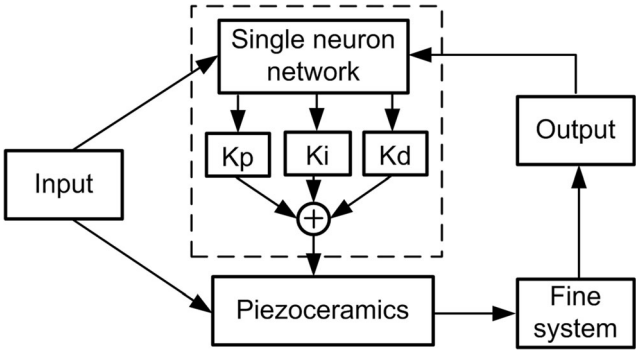

Fig. 5 The diagram of the single-neuron-based PID controller

The coarse positioning system is an open-loop system and the drive chain is long. The final accuracy of the grating ruling engine largely depends on the fine positioning system. Figure 6 presents the step response of the whole positioning system with the single-neuron-based PID controller. The response speed of the coarse system is relatively slow and the controller only contributes in the fine positioning process. Apparently, the positioning error controlled by the single-neuron-based PID controller is less than 12 nm.

Owning to the specific working mode of the grating ruling engine, the precise positioning stage should move for certain distance then stop and wait for the ruling system to rule one line of grating. Therefore, the speed requirement of the positioning system is relatively low. The bi-direction step experiment is conducted with the step time being 1 s and the step distance being 10 nm. As shown in Fig. 7, the resolution of both the two directions is higher than 10 nm. The positioning error is large in the initial period of each stepping and relatively small in the subsequent period.

In order to analyze the frequency characteristic of the positioning system, the white noise with range of ±2000 nm is

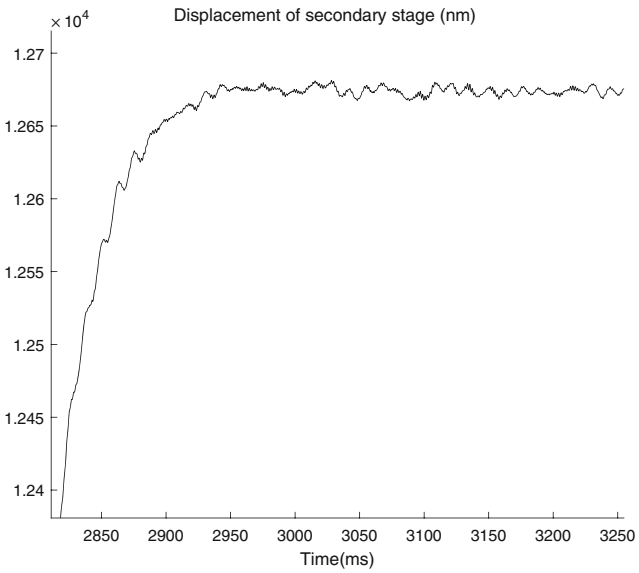

Fig. 6 The step response of the whole positioning system

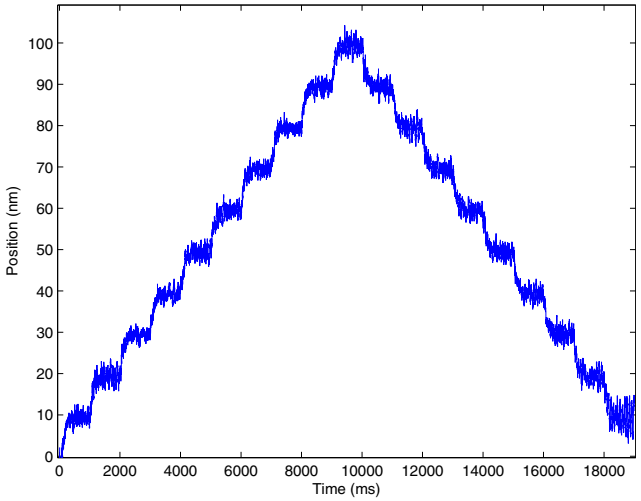

Fig. 7 The bi-direction step positioning experiment

employed to drive the piezo-actuator of the positioning stage. The spectrum analysis of the position data is presented in Fig. 8. The peak value of the spectrum analysis is about 85 Hz, which always exists in other positioning experiments with different conditions. It leads to the conclusion that the natural frequency of the positioning system is about 85 Hz. For the purpose of ensuring running stability, the control frequency and the driving frequency must be far from the natural frequency and the multiplying frequency. The control frequency of the positioning system is 1 KHz, and the driving frequency of the coarse system is less than 1 Hz. Therefore, the running stability of the positioning system is unaffected.

4 Experiment

In this section, the ruling experiment of the grating ruling engine is implemented. The first step of the ruling process is positioning. The ruling operation is carried out in the stable period of the positioning. Therefore, in the ruling experiment, the working mode of the positioning system is continuous stepping.

The function of the grating ruling engine is ruling varisized grating due to the user's requirement. According to different grating sizes, the locating modes of the positioning system are divided into the long-travel mode and the short-travel mode. The grating ruling experiments conducted in both the two modes are described as follows. In the ruling experiments, the positioning stage moves step by step. Owning to the ruling operation between two steps of the position system, the locating speed is slower than the other positioning stage.

4.1 The long-travel mode

The long-travel positioning is accomplished coordinately by the coarse system and the fine system. The positioning range of the

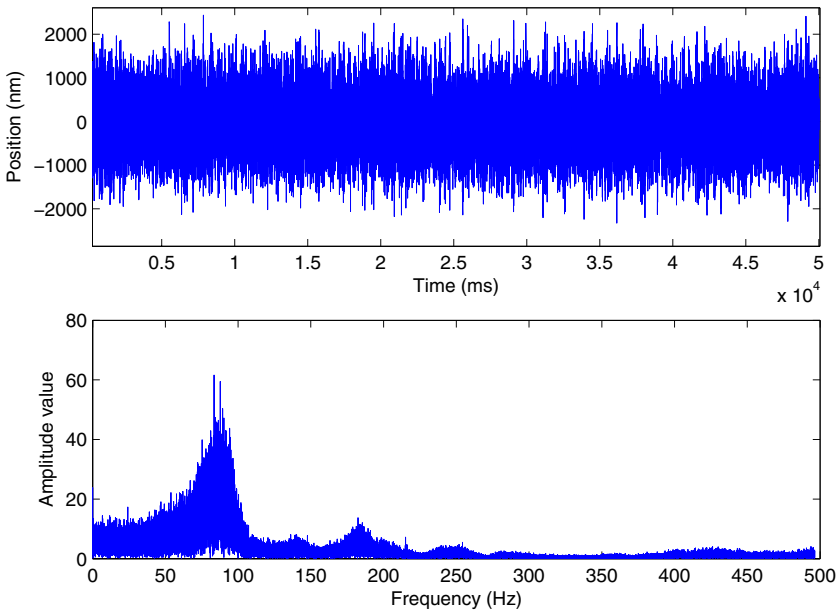

Fig. 8 The position of one step and the spectrum analysis result

long-travel mode is as long as 500 mm. The positioning process is composed of the coarse positioning and the fine positioning. Firstly, the primary stage is driven by the motor to complete the coarse positioning process. After the coarse positioning, the fine positioning process is performed by the secondary stage with the piezoelectric actuator and the control system. The fine positioning process contains an initial period and a stable period. The duration ratio of the coarse positioning, the initial period of the fine positioning, and the stable period of the fine positioning is 1:2:3 in each step. As the first two periods being preliminary periods, the last period is the one with the highest accuracy and the ruling operation is done in this period.

The positioning speed of the long-travel mode can be freely set. The positioning speed in this experiment is one step in 1 minute. The step signal with amplitude of 1/79 mm and step count of 790 is employed into the positioning stage. The total travel is 10 mm and the experiment takes 13 h in all.

Figure 9 presents the output data from step 5 to step 10 of the long-travel experiment. The blue line in Fig. 9a illustrates the coarse positioning. And the red and black lines correspond to the initial period and the stable period of the fine positioning, respectively.

As the red part of Fig. 9b shows, the piezoelectric actuator has great variation amplitude in the initial period of the fine positioning. As presented by the black part of Fig. 9b, the variation range of the piezo-actuator is smaller in the stable period, so the positioning precision of the stable period is higher than the initial period. The ruling operation is done in the stable period. Fig. 9c shows the deviations of the stable period in stepper 7, the three-sigma value of the deviations is 7.7 nm.

For comparison, Fig. 10 presents the output from step 710 to step 715 of the same positioning experiment, namely the accumulative trip is about 9 mm. The maximum length of the piezoelectric actuator in Fig. 10b is 5.1 μm, which is significantly larger than the one in Fig. 10b 30 μm. Figure 10c shows the deviations of the stable period in stepper 712, the three-sigma value of the deviations is 8.9 nm. Although the amplitude of the piezo-actuator is bigger in the later step, it is still within the normal travel range of the piezo-actuator and the positioning precision shows little change.

a) The displacement of the secondary stage
b) The length of the piezo-actuator
c) The deviations of step 712

4.2 The short-travel mode

In the short-travel mode, the positioning process is accomplished by the fine system and nothing about the coarse system. The travel range of the short-travel mode is limited to 120 μm, which is the motion range of the piezo-actuator. The step signal with amplitude of 500 nm and duration of 20 s is employed into the fine system. The output of the short-travel experiments is presented in Fig. 11.

a) The displacement and the length of piezo-actuator.
b) The displacement and deviations of step 4.

As shown in Fig. 11a, the output of the piezo-actuator in the short-travel mode is stepped, different from the saw-toothed wave in the long-travel mode. That is because without the coarse positioning process,

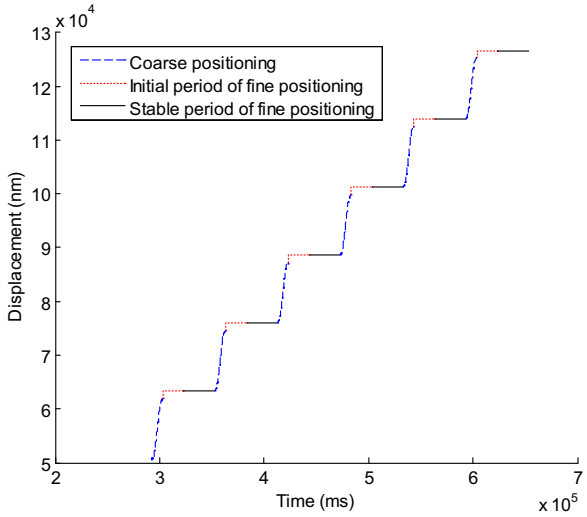

(a) The displacement of the secondary stage

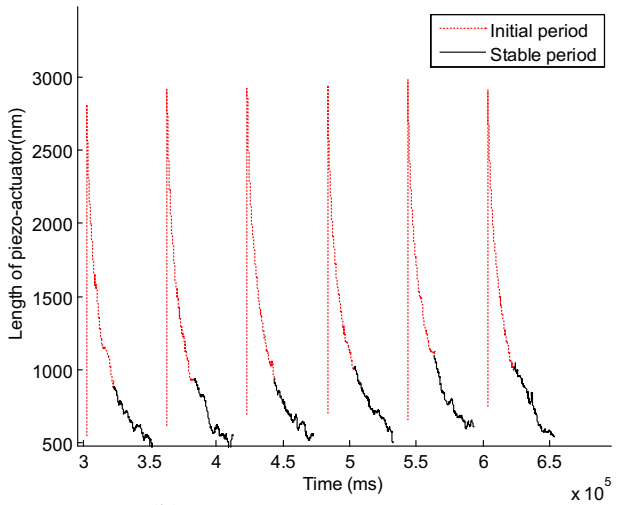

(b) The length of the piezo-actuator

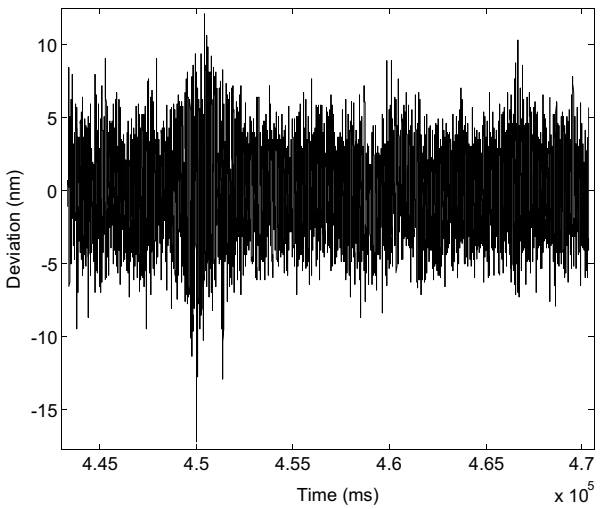

(c) The deviations of step 7

Fig. 9 The output from step 5 to step 10 of the long-travel positioning experiment

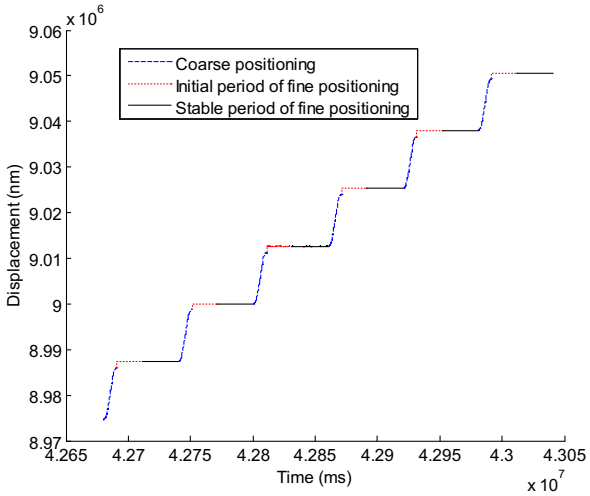

(a) The displacement of the secondary stage

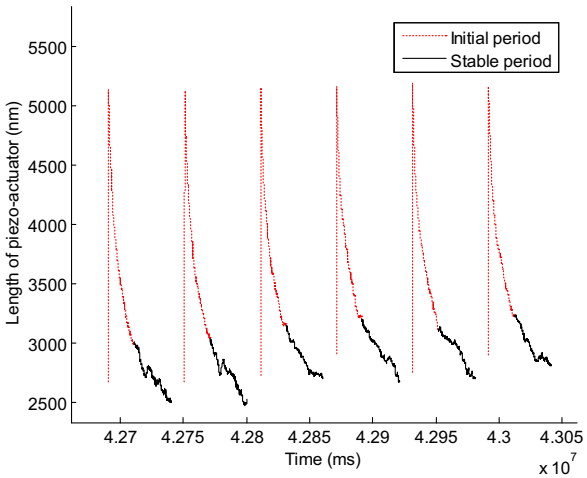

(b) The length of the piezo-actuator

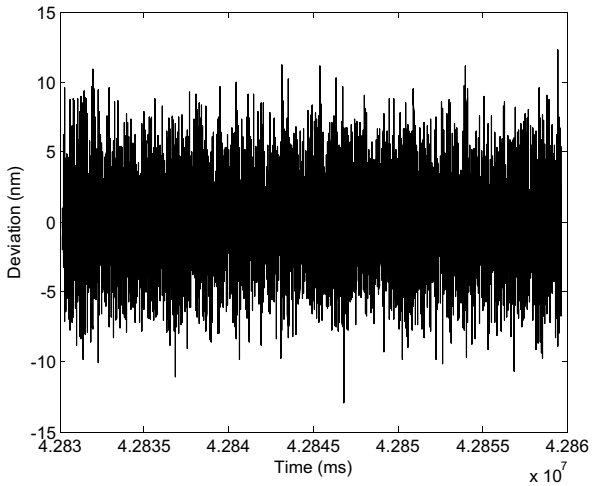

(c) The deviations of step 712

Fig. 10 The output from step 710 to step 715 of the long-travel positioning

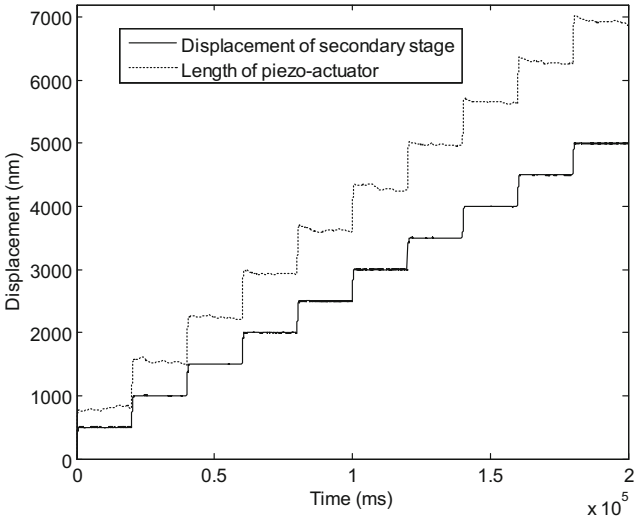

(a) The displacement and the length of piezo-actuator

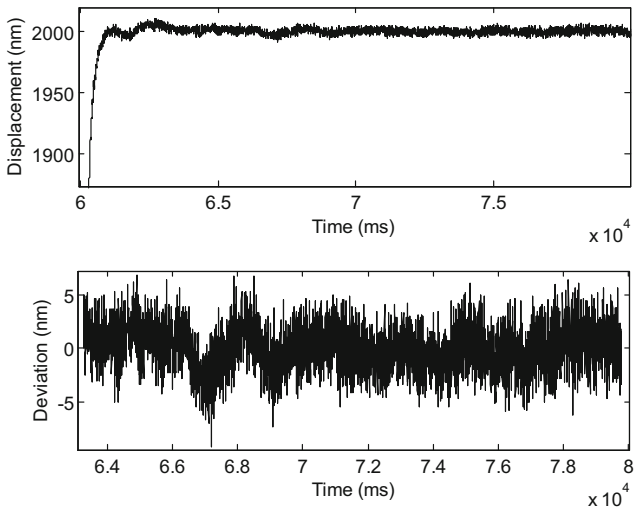

(b) The displacement and deviations of step 4

Fig. 11 The output of the short-travel locating experiment

all the output displacement is driven by the piezo-actuator, so the wave of the piezo-actuator is similar to the displacement curve of the secondary stage.

Since the piezoelectric actuator is installed between the two stages and the primary system is not a rigid body, the elongation of the piezo-actuator leads to not only the displacement of the secondary stage but also the movement of the primary stage along the reversed direction of the secondary stage. Therefore, the length of the piezo-actuator is larger than the absolute displacement of the secondary stage, as shown in Fig. 11a.

With the control frequency of 1 KHz and the quick response of the piezo-actuator, the short-travel positioning process stabilizes soon. Figure 11b displays the displacement of the step 4 and the deviations. The displacement of the secondary stage is stable within 2 s, and the three-sigma value of the deviations is 6.2 nm. The positioning precision of the short-travel mode is higher than the long-travel mode.

The position precision of both the long-travel mode and the short-travel mode can achieve 10 nm. The differences are the travel range and the positioning speed. The user can choose either mode depending upon the needs.

5 Discussions

5.1 The compensating length of the piezo-actuator

According to Fig. 9b, the length of the piezo-actuator is as long as 3 μm in the long-travel mode. Then, the source of the 3 μm is analyzed in this section. The step distance of the long-travel mode is 1/79 mm, namely 12.6 μm, and the theoretical resolution of the coarse positioning system is 1.667 μm. However, as a pure mechanical open-loop system, the resolution of the coarse system cannot meet the theoretical value and the positioning error is inevitable. Meanwhile, the coarse system is not a rigid-perfectly body and the response speed of the coarse system is relatively slow. The coarse positioning is not completely finished when the fine positioning starts. For the above reasons, there is a certain gap between the position of the secondary stage and the target location when the fine positioning begins. As shown in Fig. 9a, at the end of the blue part, the gap is about 1 μm. Meanwhile, the fine system driven by piezo-actuator is a rapid response system. So the fine system will quickly compensate the positioning error and push the secondary stage to the target location.

Another source of the 3 μm is the clearance in the machinery of the coarse system, including the screw-nut pair, worm-gear pair, and the guide rail. The release time of the clearance is longer than the duration of the coarse positioning. The piezo-actuator needs to compensate the unreleased clearance during the fine positioning. Therefore, the length of the piezo-actuator decreases along with the release of the clearance. The variation range of the length in both Figs. 9b and 10b is about 3 μm.

The maximum length of the piezo-actuator in Fig. 10b is 5.1 μm, which is significantly larger than the one in Fig. 9b 3.0 μm. That is because the clearance of the coarse system cannot release absolutely in each step and the residual clearances gradually accumulate in latter steps. Although the amplitude of the piezo-actuator is bigger in the later steps, there are little differences between the accuracy of Figs. 9c and 10c.

5.2 The positioning error

The experiment of the short-travel mode indicates that the positioning error of the ruling engine is 6.2 nm. The fine

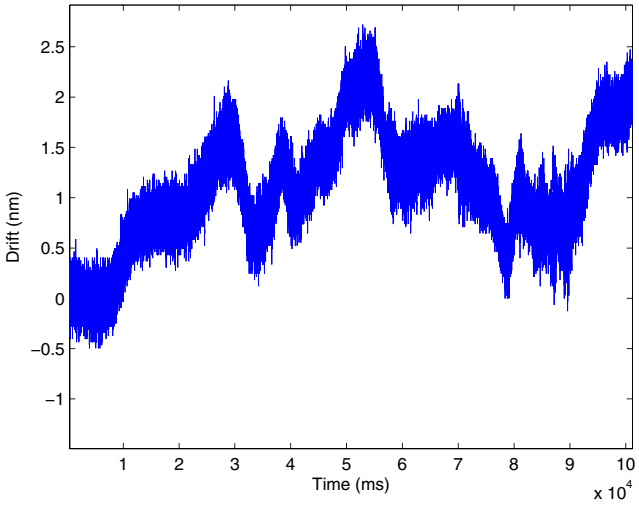

Fig. 12 The drift of the dual frequency laser interferometer

positioning system is driven by the piezo-actuator, the open-loop resolution of which is 0.15 nm, and the control frequency is 1 KHz. Therefore, the theoretically positioning accuracy of the short-travel mode is much higher. The error sources of the 6.2 nm are analyzed in this section.

There are many factors that influence the accuracy of the grating ruling engine. The first one is the measurement error. The real-time position of the secondary stage is measured by the dual-frequency laser interferometer and sent to the controller system, so the measurement error directly affects the measuring result and the control effectiveness. As shown in Fig. 12, the drift of the laser interferometer is about 3 nm during 1 minute. Despite the theoretical resolution of the interferometer being 0.15 nm, the actual resolution of the laser interferometer is less due to the drift.

Other than the measurement error, the vibration is another source of the 6.2 nm. Figure 13 presents the positioning error of the grating ruling engine during 4 days. It is obvious that the positioning error is relatively bigger during the daytime, especially in the rush hours. Meanwhile, the positioning error is relatively smaller during the nighttime. This illustrates that the vibration isolation measures are not perfect and the vibration obviously influences the positioning accuracy of the grating ruling engine.

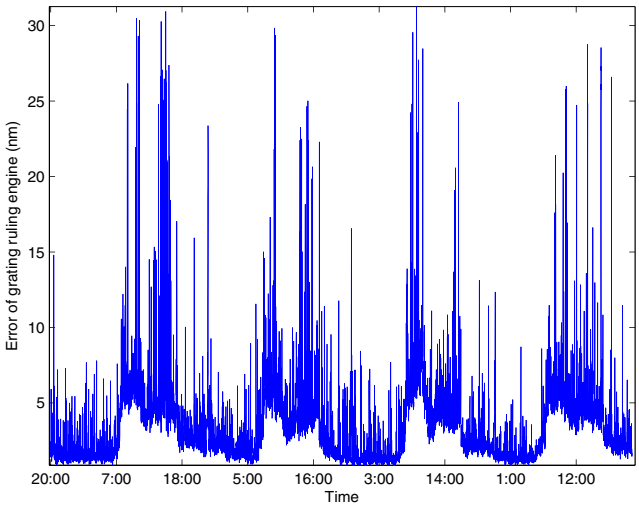

Fig. 13 The error of the grating ruling engine during 4 days

In future research, the measurement error and the vibration, which effectively influence the positioning accuracy, will be studied in detail to improve the precision of the grating ruling engine.

6 Conclusions

This paper presents a dual-drive long-travel precise positioning stage employed in the grating ruling engine. The primary stage driven by the ball screw is utilized to obtain a large travel range. The secondary stage with a closed-loop control system is designed to ensure high positioning precision. The different running modes of the system including the long-travel mode and the short-travel mode have been introduced and experimented. The results prove that the precise positioning stage of the grating ruling engine is characterized by high locating accuracy and extended travel range. The main sources of the positioning error are the shifting error of the interferometer and the external vibration. The further research will make an in-deep study of the factors to improve the positioning accuracy.

Acknowledgements This work was supported by Chongqing Municipal Educational Commission (KJ1400936), Chongqing Science and Technology Commission (cstc2016jcyjA1613), and Ministry of National Science and Technology for National Key Basic Research Program of China (2014CB049500).

References

1. Korayem MH, Zakeri M (2009) Sensitivity analysis of nanoparticles pushing critical conditions in 2-D controlled nanomanipulation based on AFM. Int J Adv Manuf Technol 41(7–8):714–726
2. Lee DY, Gweon DG (2009) Accurate measurement of the out-of-plane motion of a tip-scanning atomic force microscope. Int J Precis Eng Manuf 10(1):119–121
3. Li Y, Bechhoefer J (2007) Feedforward control of a closed-loop piezoelectric translation stage for atomic force microscope. Rev Sci Instrum 78(1):013702
4. Bosetti P, Bruschi S (2012) Enhancing positioning accuracy of CNC machine tools by means of direct measurement of deformation. Int J Adv Manuf Technol 58(5–8):651–662
5. Rakuff S, Cuttino JF (2009) Design and testing of a long-range, precision fast tool servo system for diamond turning. Precis Eng 33(1):18–25
6. Deng C, Xie SQ, Wu J, Shao XY (2014) Position error compensation of semi-closed loop servo system using support vector regression and fuzzy PID control. Int J Adv Manuf Technol 71(5–8):887–898

7. Lee CW, Kim SW (1997) An ultraprecision stage for aligment of wafers in advanced microlithography. Precis Eng 21(2–3):113–122
8. Fan KC, Lai ZF (2008) An intelligent nano-positoning control system driven by an ultrasonic motor. Int J Precis Eng Manuf 9(3):40–45
9. Chang SH, Li SS (1999) A high resolution long travel friction-drive micropositionger with programmable step size. Rev Sci Instrum 70(6):2776–2782
10. Kim SC, Kim SH (2001) A precision linear actuator using piezoelectrically driven friction force. Mechatronics 11(8):969–985
11. Liu YJ, Li T, Sun LN (2009) Design of a control system for a macro-micro dual-drive high acceleration high precision positioning stage for IC packaging. Sci China Ser E 52(7):1858–1865
12. Ito K, Takigawa N, Yamamoto M, Iwasaki M, Matsui N (2008) Online parameter tuning of disturbance compensation in precision positioning. Proc 10th IEEE Int Worksh Adv Control 26-28:672–676
13. Cheng F, Fan KC, Miao JW, Li BK, Wang HY (2012) A BPNN-PID based long-stroke nanopositioning control scheme driven by ultrasonic motor. Precis Eng 36(3):485–493
14. Liu CH, Jywe WY, Jeng YR, Hsu TH, Li YT (2010) Design and control of a long-traveling nano-positioning stage. Precis Eng 34(3):497–506
15. Li ZH, Fan KG, Yang JG, Zhang Y (2014) Time-varying positioning error modeling and compensation for ball screw systems based on simulation and experimental analysis. Int J Adv Manuf Technol 73(5–8):773–782
16. Shiau TN, Chen KH, Wang FC, Chio CT, Hsu WC (2010) The effect of dynamic behavior on surface roughness of ball screw under the grinding force. Int J Adv Manuf Technol 52(5–8):507–520
17. Chu CL, Fan SH (2006) A novel long-travel piezoelectric-driven linear nanopositioning stage. Precis Eng 30(1):85–95
18. Hwang D, Lee MG, Jeong J (2011) Note: design of a novel ultraprecision in-plane XYθ positioning stage. Rev Sci Instrum 82(2):026102
19. Zheng J, Salton A, Fu M (2011) Design and control of a rotary dual-stage actuator positioning system. Mechatronics 21(6):1003–1012
20. Yong YK, Aphale SS, Reza Moheimani SO (2009) Design, identification, and control of a flexure-based XY stage for fast nanoscale positioning. IEEE Trans Nanotechnol 8(1):46–54
21. Sundararaman KA, Guharaja S, Padmanaban KP, Sabareeswaran M (2014) Design and optimization of machining fixture layout for end-milling operation. Int J Adv Manuf Technol 73(5–8):669–679
22. Ke XL, Huang HB, Liu JC (2013) Study and application on vibration monitoring technique of precision grinding. J Chongqing Univ Technol (Nat Sci) 27(12):77–81